7 Displacement of Reference Points (25 November 2006)

Models describing the displacements of reference points due to various effects are provided. These models relate the regularized position $X_R(t)$ of the reference points (see Chapter 4) to their instantaneous positions. Two kinds of displacements are distinguished: those that affect the reference markers on the crust and those that affect the reference points of the instruments, which are technique-dependent. The first category includes (a) deformations of the solid Earth due to ocean tidal loading as well as those due to the body tides arising from the direct effect of the external tide generating potential and centrifugal perturbations caused by Earth rotation variations, including the pole tide, (b) atmospheric loading. The second category presently only includes the thermal deformation of a VLBI antenna.

7.1 Displacement of Reference Markers on the Crust

7.1.1 Local Site Displacement due to Ocean Loading

Ocean tides cause a temporal variation of the ocean mass distribution and the associated load on the crust and produce time-varying deformations of the Earth that can reach 100 mm. The modeling of the associated site displacements is dealt with in this section.

Note on motion of the center of mass of the solid Earth

When the solid Earth and fluid masses are considered as a system without any external forces acting upon it, the position of the common center of mass remains fixed in space. When a phenomenon, such as the ocean tides, causes displacements of fluid masses, the center of mass of the fluid masses moves periodically and must be compensated by an opposite motion of the center of mass of the solid Earth. The stations, being fixed to the solid Earth, are subject to this counter-motion.

For observing techniques that rely upon the dynamical motions of satellites, which respond to the center of mass of the total Earth system, the modeled motions of crust-fixed stations should include the "geocenter motion" contributions that counterbalance the effects of the fluid components. For other observing techniques, such as VLBI, neglect of geocenter motion should have no observable consequences.

Models for ocean tidal loading

The tide generating potential due to the gravitational attraction of the Moon and Sun can be described by an expansion into a set of tidal harmonics (*e.g.* Hartmann and Wenzel, 1995; Tamura, 1987; Cartwright and Tayler, 1971; Cartwright and Edden, 1973). The response of the oceans, unlike for the solid Earth, is strongly dependent on local and regional conditions that affect fluid flow. Closed-form analytical expressions are not adequate to describe the ocean tidal response globally. Instead, gridded formulations are needed. Table 7.1 lists the leading global ocean tidal models that have been developed since Schwiderski and Szeto (1981). Most modern models assimilate sea surface height measurements made by altimetry satellites.

The crustal loading at a particular location due to a given tidal harmonic is computed by integrating the tide height with a weighting function (Green's function, see Farrell, 1972), carrying the integration over all the ocean masses. The total loading may be obtained by summing the effect of all harmonics. In practice, the three-dimensional site displacements due to ocean tidal loading are computed using the following scheme. Let Δc denote a displacement component (radial, west, south) at a particular site and time t. Δc is obtained as

$$\Delta c = \sum_j A_{cj} \cos(\chi_j(t) - \phi_{cj}), \tag{1}$$

where the summation is carried out for a set of tidal constituents. The amplitudes A_{cj} and phases ϕ_{cj} describe the loading response for the chosen site. The astronomical argument $\chi_j(t)$ for the 11 main tides can be computed with the subroutine ARG.f, which can be obtained at <[1]>.

[1] ftp://tai.bipm.org/iers/convupdt/chapter7

Conventionally, only a discrete set of harmonics in the long-period ($m = 0$), diurnal ($m = 1$) and semidiurnal ($m = 2$) bands are usually considered explicitly. The 11 main tides considered are the semidiurnal waves M_2, S_2, N_2, K_2, the diurnal waves K_1, O_1, P_1, Q_1, and the long-period waves M_f, M_m, and S_{sa}. The site-dependent amplitudes A_{cj} and phases ϕ_{cj} for these 11 tides are obtained as described in the next sub-section. Amplitudes and phases for other tidal constituents can be obtained from those for the 11 main tides by a variety of approximation schemes. For instance, if one wishes to include the effect of sidelobes of the main tides generated by modulation with the 18.6-year lunar node, then suitable adjustments in the 11 amplitudes and phases can be applied so that

$$\Delta c = \sum_{k=1}^{11} f_k A_{ck} \cos(\chi_k(t) + u_k - \phi_{ck}), \tag{2}$$

where f_k and u_k depend on the longitude of the lunar node. See Scherneck (1999) for the expression of these arguments.

In more complete methods, the lesser tides are handled by interpolation of the admittances using some full tidal potential development (*e.g.* Hartmann and Wenzel, 1995). One of these methods has been chosen as the conventional IERS method, and has been implemented in a subroutine that is recommended as a conventional computation of the loading displacement (see sub-section **Conventional routine to compute the ocean loading displacement** below).

Note that complete neglect of the minor tides and nodal modulations, using (1) with only the 11 main tides, is not recommended and may lead to errors of several mm, up to 5 mm rms at high latitudes (Hugentobler, 2006).

Additional contributions to ocean-induced displacement arise from the frequency dependence of the load Love numbers due to the Nearly Diurnal Free Wobble in the diurnal tidal band. The effect of this dependence has been taken into account, following Wahr and Sasao (1981), by incrementing the *body tide* Love numbers as explained in section 7.1.2.

Site-dependent tidal coefficients

For a given site, the amplitudes A_{cj} and phases $\phi_{cj}, 1 \leq j \leq 11$, for the 11 main tides may be obtained electronically from the ocean loading service site at <[2]>; see Scherneck (1991). They are provided in either the so-called BLQ format or in the HARPOS format. An example of the BLQ format is given in Table 7.2. Note that tangential displacements are to be taken positive in west and south directions. The service allows coefficients to be computed selectably from any of fourteen ocean tide models; see Table 7.1.

The accuracy of the ocean tide loading values depends on the errors in the ocean tide models, the errors in the Green's function, the coastline representation and the numerical scheme of the loading computation itself. To have a correct representation of the water areas one normally uses a high resolution coastline of around 600 metres to 2 km. Note that still some problems exists near Antarctica where one should use the real land coastline instead of the ice shelve edges. Different elastic Earth models produce different Green's functions but their differences are small, less than 2%. Most numerical schemes to compute the loading are good to about 2-5%. Currently, the largest contributor to the uncertainty in the loading value are the errors in the ocean tide models. Therefore it is recommended to use the most recent ocean tide models (TPXO.6.2, see <[3]> for a solution derived using tide gauge and TOPEX/Poseidon data; FES2004 for a hydrodynamic solution with altimetry data). However, older models might sometimes be preferred for internal consistency. Since many space geodesy stations are inland or near coasts, the accuracy of the tide models in the shelf areas is more crucial than in the open sea. Load convolution adopts land-sea masking according to the high resolution coastlines dataset included in the Generic Mapping Tools (GMT, Wessel and Smith, 1998). Ocean tide mass budgets have been constrained using a uniform co-oscillation oceanic layer. The integrating loading kernel employs a disk-generating Green's function method (Farrell, 1972; Zschau, 1983; Scherneck, 1990).

[2] http://www.oso.chalmers.se/∼loading
[3] http://www.coas.oregonstate.edu/research/po/research/tide/global.html

When generating tables of amplitudes and phases using the ocean loading service, one has to answer the question "Do you want to correct your loading values for the [geocenter] motion?"

Answering "No" means that the coefficients do not include the large-scale effect of the geocenter motion caused by the ocean tide. This is appropriate for station coordinates given in a "crust-fixed" frame that is not sensitive to the Earth's center of mass.

Answering "Yes" means that the coefficients include the large-scale effect of the geocenter motion caused by the ocean tide. This is consistent with data analyses that realize a near-instantaneous "center of mass" frame using observations of satellite dynamics.

Table 7.1 Ocean tide models available at the automatic loading service.

Model code	Reference	Input	Resolution
SCHW	Schwiderski and Szeto (1981)	Tide gauge	$1^\circ \times 1^\circ$
CSR3.0, CSR4.0	Eanes (1994)	Topex/Poseidon Altim.	$1^\circ \times 1^\circ$
	Eanes and Bettadpur (1995)	T/P + LEPR loading	$0.5^\circ \times 0.5^\circ$
TPXO.5	Egbert *et al.* (1994)	inverse hydrodyn, solution from T/P Altim.	256×512
TPXO.6.2	Egbert *et al.* (2002) see $< {}^3 >$	idem	$0.25^\circ \times 0.25^\circ$
TPXO.7.0	pre-release, see $< {}^3 >$	idem	$0.25^\circ \times 0.25^\circ$
FES94 (LEPR)	Le Provost *et al.* (1994)	numerical model	$0.5^\circ \times 0.5^\circ$
FES95.2	Le Provost *et al.* (1998)	num. model + assim. Altim.	$0.5^\circ \times 0.5^\circ$
FES98	Lefèvre *et al.* (2000)	num. model + assim. tide gauges	$0.25^\circ \times 0.25^\circ$
FES99	Lefèvre *et al.* (2002)	numerical model + assim. tide gauges and Altim.	$0.25^\circ \times 0.25^\circ$
FES2004	Letellier (2004)	numerical model	$0.125^\circ \times 0.125^\circ$
GOT99.2, GOT00.2	Ray (1999)	T/P	$0.5^\circ \times 0.5^\circ$
NAO99.b	Matsumoto *et al.* (2000)	num. + T/P assim.	$0.5^\circ \times 0.5^\circ$

Table 7.2 Sample of ocean loading table file. Each site record shows a header with the site name, the CDP monument number, geographic coordinates and comments. First three rows of numbers designate amplitudes (meter), radial, west, south, followed by three lines with the corresponding phase values (degrees).

Columns designate partial tides $M_2, S_2, N_2, K_2, K_1, O_1, P_1, Q_1, M_f, M_m$, and S_{sa}.

```
$$
  ONSALA60 7213
$$
$$ Computed by H.G. Scherneck, Uppsala University, 1989
$$ ONSALA 7213    lon/lat: 11.9263 57.3947
.00384   .00091   .00084   .00019   .00224   .00120   .00071   .00003   .00084   .00063   .00057
.00124   .00034   .00031   .00009   .00042   .00041   .00015   .00006   .00018   .00010   .00010
.00058   .00027   .00021   .00008   .00032   .00017   .00009   .00004   .00007   .00001   .00020
  -56.0    -46.1    -90.7    -34.4    -44.5   -123.2    -49.6    178.4     14.9     37.3     24.6
   75.4     97.6     40.8     94.8    119.0     25.4     98.7    -14.1   -177.0   -126.7   -175.8
   84.2    131.3     77.7    103.9     17.2    -55.0     25.2   -165.0    173.3    121.8     91.3
```

Conventional routine to compute the ocean loading displacement

D. Agnew has provided a Fortran program (hardisp.f) to compute the ocean tide loading displacements for a site, given the amplitude A_{cj} and phases $\phi_{cj}, 1 \leq j \leq 11$, as generated by the Bos-Scherneck website (in BLQ format, see above). The implementation considers a total of 141 constituent tides whose amplitudes and phases are found by spline interpolation of the tidal admittances based on the 11 main tides. Comparisons with the ETERNA software of Wenzel (1996)

have been carried out by M. Bos (2005), who concludes that the routine is precise to about 1%. In addition, tests have been carried out using 337 constituent tides in hardisp.f instead of 141, resulting in differences of order 0.1 mm rms. Uncertainties in the ocean models are generally larger. The code for the routine can be obtained at <[1]>.

Center of mass correction

If necessary, the crust-frame translation (geocenter motion) due to the ocean tidal mass, dX(t), dY(t), and dZ(t), may be computed according to the method given by Scherneck at <[4]>, e.g. for dX(t) as

$$dX(t) = \sum_{k=1}^{11} X_{in}(k)\cos(\chi_k(t)) + X_{cr}(k)\sin(\chi_k(t)) \tag{3}$$

where the in-phase ($_{in}$) and cross-phase ($_{cr}$) amplitudes (in meters) are tabulated for the various ocean models. Similarly for dY(t) and dZ(t). This correction should be applied, for instance, in the transformation of GPS orbits from the center-of-mass to the crust-fixed frame expected in sp3 format

$$X_{crust-fixed} = X_{center-of-mass} - dX, \tag{4}$$

i.e. the translation vector should be substracted when going from center-of-mass to sp3.

7.1.2 Effects of the Solid Earth Tides

Site displacements caused by tides of spherical harmonic degree and order (nm) are characterized by the Love number h_{nm} and the Shida number l_{nm}. The effective values of these numbers depend on station latitude and tidal frequency (Wahr, 1981). The latitude dependence and a small interband variation are caused by the Earth's ellipticity and the Coriolis force due to Earth rotation. A strong frequency dependence within the diurnal band is produced by the Nearly Diurnal Free Wobble resonance associated with the free core nutation (FCN) in the wobbles of the Earth and its core regions which contribute to the tidal deformations via their centrifugal effects. Additionally, the resonance in the deformation due to ocean tidal loading, which is not included in the computations of the last section which use constant load Love numbers, may be represented in terms of effective contributions to h_{21} and l_{21}. A further frequency dependence, which is most pronounced in the long-period tidal band, arises from mantle anelasticity leading to corrections to the elastic Earth Love numbers. The contributions to the Love number parameters from anelasticity and ocean tidal loading as well as those from the centrifugal perturbations due to the wobbles have imaginary parts which cause the tidal displacements to lag slightly behind the tide generating potential. All these effects need to be taken into account when an accuracy of 1 mm is desired in determining station positions.

In order to account for the latitude dependence of the effective Love and Shida numbers, the representation in terms of multiple h and l parameters employed by Mathews *et al.* (1995) is used. In this representation, parameters $h^{(0)}$ and $l^{(0)}$ play the roles of h_{2m} and l_{2m}, while the latitude dependence is expressed in terms of additional parameters $h^{(2)}, h'$ and $l^{(1)}, l^{(2)}, l'$. These parameters are defined through their contributions to the site displacement as given by equations (5) below. Their numerical values as listed in the Conventions 1996 have since been revised, and the new values presented in Table 7.4 are used here. These values pertain to the elastic Earth and anelasticity models referred to in Chapter 6.

The vector displacement due to a tidal term of frequency f is given in terms of the several parameters by the following expressions that result from evaluation of the defining equation (6) of Mathews *et al.* (1995):

[4] http://www.oso.chalmers.se/∼loading/cmc.html

For a long-period tide of frequency f:

$$\begin{aligned}\Delta\vec{r}_f &= \sqrt{\tfrac{5}{4\pi}}H_f \quad \Big\{ \quad \Big[h(\phi)\left(\tfrac{3}{2}\sin^2\phi - \tfrac{1}{2}\right) + \sqrt{\tfrac{4\pi}{5}}h'\Big]\cos\theta_f\ \hat{r} \\ &\qquad +3l(\phi)\sin\phi\cos\phi\cos\theta_f\ \hat{n} \\ &\qquad +\cos\phi\ \Big[3l^{(1)}\sin^2\phi - \sqrt{\tfrac{4\pi}{5}}l'\Big]\sin\theta_f\ \hat{e}\Big\}.\end{aligned} \tag{5a}$$

For a diurnal tide of frequency f:

$$\begin{aligned}\Delta\vec{r}_f &= -\sqrt{\tfrac{5}{24\pi}}H_f \quad \Big\{h(\phi)3\sin\phi\cos\phi\sin(\theta_f+\lambda)\ \hat{r} \\ &+\Big[3l(\phi)\cos 2\phi - 3l^{(1)}\sin^2\phi + \sqrt{\tfrac{24\pi}{5}}l'\Big]\sin(\theta_f+\lambda)\ \hat{n} \\ &+\Big[\Big(3l(\phi) - \sqrt{\tfrac{24\pi}{5}}l'\Big)\sin\phi - 3l^{(1)}\sin\phi\cos 2\phi\Big]\cos(\theta_f+\lambda)\ \hat{e}\Big\}\ .\end{aligned} \tag{5b}$$

For a semidiurnal tide of frequency f:

$$\begin{aligned}\Delta\vec{r}_f &= \sqrt{\tfrac{5}{96\pi}}H_f\{ \quad [h(\phi)3\cos^2\phi\cos(\theta_f+2\lambda)\ \hat{r} \\ &\qquad -6\sin\phi\cos\phi[l(\phi)+l^{(1)}]\cos(\theta_f+2\lambda)\ \hat{n} \\ &\qquad -6\cos\phi[l(\phi)+l^{(1)}\sin^2\phi]\sin(\theta_f+2\lambda)\ \hat{e}\}.\end{aligned} \tag{5c}$$

In the above expressions,

$$\begin{aligned}h(\phi) &= h^{(0)} + h^{(2)}[(3/2)\sin^2\phi - 1/2], \\ l(\phi) &= l^{(0)} + l^{(2)}[(3/2)\sin^2\phi - 1/2],\end{aligned} \tag{6}$$

H_f = amplitude (m) of the tidal term of frequency f,

ϕ = geocentric latitude of station,

λ = east longitude of station,

θ_f = tide argument for tidal constituent with frequency f,

$\hat{r}$ = unit vector in the radial direction,

$\hat{e}$ = unit vector in the east direction,

$\hat{n}$ = unit vector at right angles to $\hat{r}$ in the northward direction.

The convention used in defining the tidal amplitude H_f is as in Cartwright and Tayler (1971). To convert amplitudes defined according to other conventions that have been employed in recent more accurate tables, use the conversion factors given in Chapter 6, Table 6.5.

Equations (5) assume that the Love and Shida number parameters are all real. Generalization to the case of complex parameters is done simply by making the following replacements for the combinations $L\cos(\theta_f + m\lambda)$ and $L\sin(\theta_f + m\lambda)$, wherever they occur in those equations:

$$L\cos(\theta_f + m\lambda) \rightarrow L^R\cos(\theta_f + m\lambda) - L^I\sin(\theta_f + m\lambda), \tag{7a}$$

$$L\sin(\theta_f + m\lambda) \rightarrow L^R\sin(\theta_f + m\lambda) + L^I\cos(\theta_f + m\lambda), \tag{7b}$$

where L is a generic symbol for $h^{(0)}, h^{(2)}, h', l^{(0)}, l^{(1)}, l^{(2)},$ and l', and L^R and L^I stand for their respective real and imaginary parts.

The complex values of these 7 parameters are computed for the diurnal body tides from resonance formulae of the form given in equation (6) of Chapter 6 using the values listed in equation (7) of that chapter for the resonance frequencies σ_α and those listed in Table 7.3 for the coefficients L_0

and L_α relating to each of the multiple h and l Love/Shida numbers. The manner in which σ_α and the L_α were computed is explained in Chapter 6, where mention is also made of the models used for the elastic Earth and for mantle anelasticity. As was noted in that chapter, the frequency dependence of the ocean tide contributions to certain Earth parameters in the equations of motion for the wobbles has the effect of making the resonance formulae inexact. The difference between the exact and resonance formula values is included in the tabulated values of $h_{21}^{(0)}$ and $l_{21}^{(0)}$ in Table 7.4. (The only case where this difference makes a contribution above the cut-off in Table 7.5a is in the radial displacement due to the ψ_1 tide.) Also included in the values listed in Table 7.4 are the resonant ocean tidal loading corrections outlined in the next paragraph.

Table 7.3 Parameters in the Resonance Formulae for the Displacement Love Numbers.

	$h^{(0)}$		$h^{(2)}$	
α	Re L_α	Im L_α	Re L_α	Im L_α
0	$0.60671 \times 10^{+0}$	-0.2420×10^{-2}	-0.615×10^{-3}	-0.122×10^{-4}
1	-0.15777×10^{-2}	-0.7630×10^{-4}	0.160×10^{-5}	0.116×10^{-6}
2	0.18053×10^{-3}	-0.6292×10^{-5}	0.201×10^{-6}	0.279×10^{-8}
3	-0.18616×10^{-5}	0.1379×10^{-6}	-0.329×10^{-7}	-0.217×10^{-8}
	$l^{(0)}$		$l^{(1)}$	
α	Re L_α	Im L_α	Re L_α	Im L_α
0	$.84963 \times 10^{-1}$	$-.7395 \times 10^{-3}$	$.121 \times 10^{-2}$	$.136 \times 10^{-6}$
1	$-.22107 \times 10^{-3}$	$-.9646 \times 10^{-5}$	$-.316 \times 10^{-5}$	$-.166 \times 10^{-6}$
2	$-.54710 \times 10^{-5}$	$-.2990 \times 10^{-6}$	$.272 \times 10^{-6}$	$-.858 \times 10^{-8}$
3	$-.29904 \times 10^{-7}$	$-.7717 \times 10^{-8}$	$-.545 \times 10^{-8}$	$.827 \times 10^{-11}$
	$l^{(2)}$		l'	
α	Re L_α	Im L_α	Re L_α	Im L_α
0	$.19334 \times 10^{-3}$	$-.3819 \times 10^{-5}$	$-.221 \times 10^{-3}$	$-.474 \times 10^{-7}$
1	$-.50331 \times 10^{-6}$	$-.1639 \times 10^{-7}$	$.576 \times 10^{-6}$	$.303 \times 10^{-7}$
2	$-.66460 \times 10^{-8}$	$.5076 \times 10^{-9}$	$.128 \times 10^{-6}$	$-.378 \times 10^{-8}$
3	$.10372 \times 10^{-7}$	$.7511 \times 10^{-9}$	$-.655 \times 10^{-8}$	$-.291 \times 10^{-9}$

Site displacements caused by solid Earth deformations due to ocean tidal loading have been dealt with in the first section of this chapter. Constant nominal values were assumed for the load Love numbers in computing these. The values used for tides of degree 2 were

$$h_2'^{(nom)} = -1.001, \quad l_2'^{(nom)} = 0.0295, \quad k_2'^{(nom)} = -0.3075.$$

Since resonances in the diurnal band cause the values of the load Love numbers too to vary, corrections need to be applied to the results of the first section. These corrections can be expressed in terms of effective ocean tide contributions $\delta h^{(OT)}$ and $\delta l^{(OT)}$ to the respective body tide Love numbers $h_{21}^{(0)}$ and $l_{21}^{(0)}$. $\delta h^{(OT)}$ and $\delta l^{(OT)}$ are given by expressions of the form (8) of Chapter 6, with appropriate replacements. They were computed using the same ocean tide admittances as in that chapter, and using the resonance parameters listed in Table 6.2 for the load Love numbers; they are included in the values listed in Table 7.4 under $h^{(0)R}$ and $h^{(0)I}$ for the diurnal tides.

The variation of $h_{20}^{(0)}$ and $l_{20}^{(0)}$ across the zonal tidal band, $(nm) = (20)$, due to mantle anelasticity, is described by the formulae

$$h_{20}^{(0)} = 0.5998 - 9.96 \times 10^{-4} \left\{ \cot \frac{\alpha\pi}{2} \left[1 - \left(\frac{f_m}{f} \right)^\alpha \right] + i \left(\frac{f_m}{f} \right)^\alpha \right\}, \tag{8a}$$

$$l_{20}^{(0)} = 0.0831 - 3.01 \times 10^{-4} \left\{ \cot \frac{\alpha\pi}{2} \left[1 - \left(\frac{f_m}{f} \right)^{\alpha} \right] + i \left(\frac{f_m}{f} \right)^{\alpha} \right\} \qquad (8b)$$

on the basis of the anelasticity model already referred to. Here f is the frequency of the zonal tidal constituent, f_m is the reference frequency equivalent to a period of 200 s, and $\alpha = 0.15$.

Table 7.4 lists the values of $h^{(0)}, h^{(2)}, h', l^{(0)}, l^{(1)}, l^{(2)}$, and l' for those tidal frequencies for which they are needed for use in the computational procedure described below. The tidal frequencies shown in the table are in cycles per sidereal day (*cpsd*). Periods, in solar days, of the nutations associated with the diurnal tides are also shown.

Computation of the variations of station coordinates due to solid Earth tides, like that of geopotential variations, is done most efficiently by the use of a two-step procedure. The evaluations in the first step use the expression in the time domain for the full degree 2 tidal potential or for the parts that pertain to particular bands ($m = 0, 1,$ or 2). Nominal values common to all the tidal constituents involved in the potential and to all stations are used for the Love and Shida numbers h_{2m} and l_{2m} in this step. They are chosen with reference to the values in Table 7.4 so as to minimize the computational effort needed in Step 2. Along with expressions for the dominant contributions from $h^{(0)}$ and $l^{(0)}$ to the tidal displacements, relatively small contributions from some of the other parameters are included in Step 1 for reasons of computational efficiency. The displacements caused by the degree 3 tides are also computed in the first step, using constant values for h_3 and l_3.

Corrections to the results of the first step are needed to take account of the frequency dependent deviations of the Love and Shida numbers from their respective nominal values, and also to compute the out-of-phase contributions from the zonal tides. Computations of these corrections constitute Step 2. The total displacement due to the tidal potential is the sum of the displacements computed in Steps 1 and 2.

The full scheme of computation is outlined in the chart on page 7.

CORRECTIONS FOR THE STATION TIDAL DISPLACEMENTS

Step 1: Corrections to be computed in the time domain

in-phase	for degree 2 and 3	Nominal values
	. for degree 2 → eq (9)	$h_2 \rightarrow h(\phi) = h^{(0)} + h^{(2)}[(3\sin^2\phi - 1)/2]$
		$l_2 \rightarrow l(\phi) = l^{(0)} + l^{(2)}[(3\sin^2\phi - 1)/2]$
		$h^{(0)} = 0.6078$, $h^{(2)} = -0.0006$; $l^{(0)} = 0.0847$, $l^{(2)} = 0.0002$
	. for degree 3 → eq (10)	$h_3 = 0.292$ and $l_3 = 0.015$
out-of-phase	for degree 2 only	Nominal values
	. diurnal tides → eq (14)	$h^I = -0.0025$ and $l^I = -0.0007$
	. semidiurnal tides → eq (15)	$h^I = -0.0022$ and $l^I = -0.0007$
contribution	from latitude dependence	Nominal values
	. diurnal tides → eq (12)	$l^{(1)} = 0.0012$
	. semidiurnal tides → eq (13)	$l^{(1)} = 0.0024$

Step 2: Corrections to be computed in the frequency domain and to be added to results of Step 1

in-phase	for degree 2	
	. diurnal tides → eqs (16)	→ Sum over all the components of Table 7.5a
	. semidiurnal tides	negligible
in-phase	and out-of-phase for degree 2	
	. long-period tides → eqs (17)	→ Sum over all the components of Table 7.5b

Displacement due to degree 2 tides, with nominal values for $h_{2m}^{(0)}$ and $l_{2m}^{(0)}$

The first stage of the Step 1 calculations employs real nominal values h_2 and l_2 common to all the degree 2 tides for the Love and Shida numbers. It is found to be computationally most

Table 7.4 Displacement Love number parameters for degree 2 tides. Superscripts R and I identify the real and imaginary parts, respectively.

Name	Period	Frequency	$h^{(0)R}$	$h^{(0)I}$	$h^{(2)}$	h'
Semidiurnal		-2 *cpsd*	.6078	-.0022	-.0006	
Diurnal						
$2Q_1$	6.86	0.85461	.6039	-.0027	-.0006	
σ_1	7.10	0.85946	.6039	-.0026	-.0006	
135,645	9.12	0.89066	.6036	-.0026	-.0006	
Q_1	9.13	0.89080	.6036	-.0026	-.0006	
ρ_1	9.56	0.89565	.6035	-.0026	-.0006	
145,545	13.63	0.92685	.6028	-.0025	-.0006	
O_1	13.66	0.92700	.6028	-.0025	-.0006	
τ_1	14.77	0.93246	.6026	-.0025	-.0006	
$N\tau_1$	23.94	0.95835	.6011	-.0024	-.0006	
NO_1	27.55	0.96381	.6005	-.0023	-.0006	
χ_1	31.81	0.96865	.5998	-.0023	-.0006	
π_1	121.75	0.99181	.5878	-.0015	-.0006	
P_1	182.62	0.99454	.5817	-.0011	-.0006	
S_1	365.26	0.99727	.5692	-.0004	-.0006	
165,545	6798.38	0.99985	.5283	.0023	-.0007	
K_1	infinity	1.00000	.5236	.0030	-.0007	
165,565	-6798.38	1.00015	.5182	.0036	-.0007	
165,575	-3399.19	1.00029	.5120	.0043	-.0007	
ψ_1	-365.26	1.00273	1.0569	.0036	-.0001	
166,564	-346.64	1.00288	.9387	-.0050	-.0003	
ϕ_1	-182.62	1.00546	.6645	-.0059	-.0006	
θ_1	-31.81	1.03135	.6117	-.0030	-.0006	
J_1	-27.55	1.03619	.6108	-.0030	-.0006	
OO_1	-13.66	1.07300	.6080	-.0028	-.0006	
Long period						
55,565	6798.38	.000147	.6344	-.0093	-.0006	.0001
S_{sa}	182.62	.005461	.6182	-.0054	-.0006	.0001
M_m	27.55	.036193	.6126	-.0041	-.0006	.0001
M_f	13.66	.073002	.6109	-.0037	-.0006	.0001
75,565	13.63	.073149	.6109	-.0037	-.0006	.0001

Name	Period	Frequency	$l^{(0)R}$	$l^{(0)I}$	$l^{(1)}$	$l^{(2)}$	l'
Semidiurnal		-2 *cpsd*	.0847	-.0007	.0024	.0002	
Diurnal							
Q_1	9.13	0.89080	.0846	-.0006	.0012	.0002	-.0002
145,545	13.63	0.92685	.0846	-.0006	.0012	.0002	-.0002
O_1	13.66	0.92700	.0846	-.0006	.0012	.0002	-.0002
NO_1	27.55	0.96381	.0847	-.0006	.0012	.0002	-.0002
P_1	182.62	0.99454	.0853	-.0006	.0012	.0002	-.0002
165,545	6798.38	0.99985	.0869	-.0006	.0011	.0002	-.0003
K_1	infinity	1.00000	.0870	-.0006	.0011	.0002	-.0003
165,565	-6798.38	1.00015	.0872	-.0006	.0011	.0002	-.0003
ψ_1	-365.26	1.00273	.0710	-.0020	.0019	.0002	.0001
ϕ_1	-182.62	1.00546	.0828	-.0007	.0013	.0002	-.0002
J_1	-27.55	1.03619	.0845	-.0006	.0012	.0002	-.0002
OO_1	-13.66	1.07300	.0846	-.0006	.0012	.0002	-.0002
Long period							
55,565	6798.38	.000147	.0936	-.0028	.0000	.0002	
S_{sa}	182.62	.005461	.0886	-.0016	.0000	.0002	
M_m	27.55	.036193	.0870	-.0012	.0000	.0002	
M_f	13.66	.073002	.0864	-.0011	.0000	.0002	
75,565	13.63	.073149	.0864	-.0011	.0000	.0002	

economical to choose these to be the values for the semidiurnal tides (which have very little intra-band variation). On using the nominal values, the vector displacement of the station due to the degree 2 tides is given by

$$\Delta\vec{r} = \sum_{j=2}^{3} \frac{GM_j R_e^4}{GM_\oplus R_j^3} \left\{ h_2\, \hat{r} \left(\frac{3}{2}(\hat{R}_j \cdot \hat{r})^2 - \frac{1}{2} \right) + 3l_2 (\hat{R}_j \cdot \hat{r})[\hat{R}_j - (\hat{R}_j \cdot \hat{r})\, \hat{r}] \right\}, \quad (9)$$

where $h_{22}^{(0)}$ and $l_{22}^{(0)}$ of the semidiurnal tides are chosen as the nominal values h_2 and l_2. The out-of-phase displacements due to the imaginary parts of the Love numbers are dealt with separately below. In equation (9),

GM_j	=	gravitational parameter for the Moon ($j = 2$) or the Sun ($j = 3$),
$GM_\oplus$	=	gravitational parameter for the Earth,
$\hat{R}_j, R_j$	=	unit vector from the geocenter to Moon or Sun and the magnitude of that vector,
R_e	=	Earth's equatorial radius,
$\hat{r}, r$	=	unit vector from the geocenter to the station and the magnitude of that vector,
h_2	=	nominal degree 2 Love number,
l_2	=	nominal degree 2 Shida number.

Note that the part proportional to h_2 gives the radial (not vertical) component of the tide-induced station displacement, and the terms in l_2 represent the vector displacement transverse to the radial direction (and not in the horizontal plane).

The computation just described may be generalized to include the latitude dependence arising through $h^{(2)}$ by simply adding $h^{(2)}[(3/2)\sin^2\phi - (1/2)]$ to the constant nominal value given above, with $h^{(2)} = -0.0006$. The addition of a similar term (with $l^{(2)} = 0.0002$) to the nominal value of l_2 takes care of the corresponding contribution to the transverse displacement. The resulting incremental displacements are small, not exceeding 0.4 mm radially and 0.2 mm in the transverse direction.

Displacements due to degree 3 tides

The Love numbers of the degree 3 tides may be taken as real and constant in computations to the degree of accuracy aimed at here. The vector displacement due to these tides is then given by

$$\Delta\vec{r} = \sum_{j=2}^{3} \frac{GM_j R_e^5}{GM_\oplus R_j^4} \left\{ h_3\, \hat{r} \left(\frac{5}{2}(\hat{R}_j \cdot \hat{r})^3 - \frac{3}{2}(\hat{R}_j \cdot \hat{r}) \right) + l_3 \left(\frac{15}{2}(\hat{R}_j \cdot \hat{r})^2 - \frac{3}{2} \right) [\hat{R}_j - (\hat{R}_j \cdot \hat{r})\hat{r}] \right\}. \quad (10)$$

Only the Moon's contribution ($j = 2$) need be computed, the term due to the Sun being negligible. The transverse part of the displacement (10) does not exceed 0.2 mm, but the radial displacement can reach 1.7 mm.

Contributions to the transverse displacement due to the $l^{(1)}$ term

The imaginary part of $l^{(1)}$ is negligible, as is the intra-band variation of Re $l^{(1)}$; and $l^{(1)}$ is effectively zero in the zonal band.

In the expressions given below, and elsewhere in this chapter,

Φ_j = body fixed geocentric latitude of Moon or Sun, and
λ_j = body fixed east longitude (from Greenwich) of Moon or Sun.

The following formulae may be employed when the use of Cartesian coordinates X_j, Y_j, Z_j of the body relative to the terrestrial reference frame is preferred:

$$P_2^0(\sin\Phi_j) = \tfrac{1}{R_j^2}\left(\tfrac{3}{2}Z_j^2 - \tfrac{1}{2}R_j^2\right), \quad (11a)$$

$$P_2^1(\sin\Phi_j)\cos\lambda_j = \tfrac{3X_jZ_j}{R_j^2},$$
$$P_2^1(\sin\Phi_j)\sin\lambda_j = \tfrac{3Y_jZ_j}{R_j^2}, \tag{11b}$$

$$P_2^2(\sin\Phi_j)\cos 2\lambda_j = \tfrac{3}{R_j^2}(X_j^2 - Y_j^2),$$
$$P_2^2(\sin\Phi_j)\sin 2\lambda_j = \tfrac{6}{R_j^2}X_jY_j. \tag{11c}$$

Contribution from the diurnal band (with $l^{(1)} = 0.0012$):

$$\delta\vec{t} = -l^{(1)}\sin\phi\sum_{j=2}^{3}\frac{GM_jR_e^4}{GM_\oplus R_j^3}P_2^1(\sin\Phi_j)[\sin\phi\cos(\lambda-\lambda_j)\ \hat{n} - \cos 2\phi\sin(\lambda-\lambda_j)\ \hat{e}]. \tag{12}$$

Contribution from the semidiurnal band (with $l^{(1)} = 0.0024$):

$$\delta\vec{t} = -\frac{1}{2}l^{(1)}\sin\phi\cos\phi\sum_{j=2}^{3}\frac{GM_jR_e^4}{GM_\oplus R_j^3}P_2^2(\sin\Phi_j)[\cos 2(\lambda-\lambda_j)\ \hat{n} + \sin\phi\sin 2(\lambda-\lambda_j)\ \hat{e}]. \tag{13}$$

The contributions of the $l^{(1)}$ term to the transverse displacements caused by the diurnal and semidiurnal tides could be up to 0.8 mm and 1.0 mm respectively.

Out of phase contributions from the imaginary parts of $h_{2m}^{(0)}$ and $l_{2m}^{(0)}$

In the following, h^I and l^I stand for the imaginary parts of $h_{2m}^{(0)}$ and $l_{2m}^{(0)}$.

Contributions δr to radial and $\delta\vec{t}$ to transverse displacements from diurnal tides (with $h^I = -0.0025$, $l^I = -0.0007$):

$$\delta r = -\frac{3}{4}h^I\sum_{j=2}^{3}\frac{GM_jR_e^4}{GM_\oplus R_j^3}\sin 2\Phi_j\sin 2\phi\sin(\lambda-\lambda_j), \tag{14a}$$

$$\delta\vec{t} = -\frac{3}{2}l^I\sum_{j=2}^{3}\frac{GM_jR_e^4}{GM_\oplus R_j^3}\sin 2\Phi_j[\cos 2\phi\sin(\lambda-\lambda_j)\ \hat{n} + \sin\phi\cos(\lambda-\lambda_j)\ \hat{e}]. \tag{14b}$$

Contributions from semidiurnal tides (with h^I=−0.0022, l^I=−0.0007):

$$\delta r = -\frac{3}{4}h^I\sum_{j=2}^{3}\frac{GM_jR_e^4}{GM_\oplus R_j^3}\cos^2\Phi_j\cos^2\phi\sin 2(\lambda-\lambda_j), \tag{15a}$$

$$\delta\vec{t} = \frac{3}{4}l^I\sum_{j=2}^{3}\frac{GM_jR_e^4}{GM_\oplus R_j^3}\cos^2\Phi_j[\sin 2\phi\sin 2(\lambda-\lambda_j)\ \hat{n} - 2\cos\phi\cos 2(\lambda-\lambda_j)\ \hat{e}]. \tag{15b}$$

The out-of-phase contributions from the zonal tides has no closed expression in the time domain.

Computations of Step 2 are to take account of the intra-band variation of $h_{2m}^{(0)}$ and $l_{2m}^{(0)}$. Variations of the imaginary parts are negligible except as stated below. For the zonal tides, however, the contributions from the imaginary part have to be computed in Step 2.

Correction for frequency dependence of the Love and Shida numbers

(a) Contributions from the diurnal band

Corrections to the radial and transverse station displacements δr and $\delta\vec{t}$ due to a diurnal tidal term of frequency f are obtainable from equation (5b):

$$\delta r \quad = \quad [\delta R_f^{(ip)}\sin(\theta_f+\lambda) + \delta R_f^{(op)}\cos(\theta_f+\lambda)]\sin 2\phi, \tag{16a}$$

$$\begin{aligned}\delta\vec{t} &= [\delta T_f^{(ip)}\cos(\theta_f+\lambda) - \delta T_f^{(op)}\sin(\theta_f+\lambda)]\sin\phi\ \hat{e} \\ &+ [\delta T_f^{(ip)}\sin(\theta_f+\lambda) + \delta T_f^{(op)}\cos(\theta_f+\lambda)]\cos 2\phi\ \hat{n},\end{aligned} \tag{16b}$$

where

$$\begin{pmatrix} \delta R_f^{(ip)} \\ \delta R_f^{(op)} \end{pmatrix} = -\tfrac{3}{2}\sqrt{\tfrac{5}{24\pi}} H_f \begin{pmatrix} \delta h_f^R \\ \delta h_f^I \end{pmatrix},$$
$$\begin{pmatrix} \delta T_f^{(ip)} \\ \delta T_f^{(op)} \end{pmatrix} = -3\sqrt{\tfrac{5}{24\pi}} H_f \begin{pmatrix} \delta l_f^R \\ \delta l_f^I \end{pmatrix}, \tag{16c}$$

and

δh_f^R and δh_f^I are the differences of $h^{(0)R}$ and $h^{(0)I}$ at frequency f from the nominal values h_2 and h^I used in equations (9) and (14a), respectively,

δl_f^R and δl_f^I are the differences of $l^{(0)R}$ and $l^{(0)I}$ at frequency f from the nominal values l_2 and l^I used in equations (9) and (14b), respectively.

Table 7.5a Corrections due to the frequency variation of Love and Shida numbers for diurnal tides. Units: mm. All terms with radial correction ≥ 0.05 mm are shown. Nominal values are $h_2 = 0.6078$ and $l_2 = 0.0847$ for the real parts, and $h^I = -0.0025$ and $l^I = -0.0007$ for the imaginary parts. Frequencies shown are in degrees per hour.

Name	Frequency	Doodson	τ	s	h	p	N'	p_s	ℓ	ℓ'	F	D	Ω	$\Delta R_f^{(ip)}$	$\Delta R_f^{(op)}$	$\Delta T_f^{(ip)}$	$\Delta T_f^{(op)}$
Q_1	13.39866	135,655	1	-2	0	1	0	0	1	0	2	0	2	-0.08	0.00	-0.01	0.01
	13.94083	145,545	1	-1	0	0	-1	0	0	0	2	0	1	-0.10	0.00	0.00	0.00
O_1	13.94303	145,555	1	-1	0	0	0	0	0	0	2	0	2	-0.51	0.00	-0.02	0.03
NO_1	14.49669	155,655	1	0	0	1	0	0	1	0	0	0	0	0.06	0.00	0.00	0.00
π_1	14.91787	162,556	1	1	-3	0	0	1	0	1	2	-2	2	-0.06	0.00	0.00	0.00
P_1	14.95893	163,555	1	1	-2	0	0	0	0	0	2	-2	2	-1.23	-0.07	0.06	0.01
	15.03886	165,545	1	1	0	0	-1	0	0	0	0	0	-1	-0.22	0.01	0.01	0.00
K_1	15.04107	165,555	1	1	0	0	0	0	0	0	0	0	0	12.00	-0.78	-0.67	-0.03
	15.04328	165,565	1	1	0	0	1	0	0	0	0	0	1	1.73	-0.12	-0.10	0.00
ψ_1	15.08214	166,554	1	1	1	0	0	-1	0	-1	0	0	0	-0.50	-0.01	0.03	0.00
ϕ_1	15.12321	167,555	1	1	2	0	0	0	0	0	-2	2	-2	-0.11	0.01	0.01	0.00

(b) Contributions from the long-period band

Corrections δr and $\delta\vec{t}$ due to a zonal tidal term of frequency f include both in-phase (ip) and out-of-phase (op) parts. From equations (5a) and (7) one finds that

$$\delta r = \left(\frac{3}{2}\sin^2\phi - \frac{1}{2}\right)(\delta R_f^{(ip)}\cos\theta_f + \delta R_f^{(op)}\sin\theta_f), \tag{17a}$$

and

$$\delta\vec{t} = (\delta T_f^{(ip)}\cos\theta_f + \delta T_f^{(op)}\sin\theta_f)\ \sin 2\phi\ \hat{n}, \tag{17b}$$

where

$$\begin{pmatrix} \delta R_f^{(ip)} \\ \delta R_f^{(op)} \end{pmatrix} = \sqrt{\tfrac{5}{4\pi}} H_f \begin{pmatrix} \delta h_f^R \\ -\delta h_f^I \end{pmatrix},$$

and

$$\begin{pmatrix} \delta T_f^{(ip)} \\ \delta T_f^{(op)} \end{pmatrix} = \tfrac{3}{2}\sqrt{\tfrac{5}{4\pi}} H_f \begin{pmatrix} \delta l_f^R \\ -\delta l_f^I \end{pmatrix}. \tag{17c}$$

Table 7.5b Corrections due to frequency variation of Love and Shida numbers for zonal tides. Units: mm. All terms with radial correction ≥ 0.05 mm are shown. Nominal values are $h = 0.6078$ and $l = 0.0847$.

Name	Frequency	Doodson	τ	s	h	p	N'	p_s	ℓ	ℓ'	F	D	Ω	$\Delta R_f^{(ip)}$	$\Delta R_f^{(op)}$	$\Delta T_f^{(ip)}$	$\Delta T_f^{(op)}$
	0.00221	55,565	0	0	0	0	1	0	0	0	0	0	1	0.47	0.16	0.23	0.07
S_{sa}	0.08214	57,555	0	0	2	0	0	0	0	0	-2	2	-2	-0.20	-0.11	-0.12	-0.05
M_m	0.54438	65,455	0	1	0	-1	0	0	-1	0	0	0	0	-0.11	-0.09	-0.08	-0.04
M_f	1.09804	75,555	0	2	0	0	0	0	0	0	-2	0	-2	-0.13	-0.15	-0.11	-0.07
	1.10024	75,565	0	2	0	0	1	0	0	0	-2	0	-1	-0.05	-0.06	-0.05	-0.03

Values of ΔR_f and ΔT_f listed in Tables 7.5a and 7.5b are for the constituents that must be taken into account to ensure an accuracy of 1 mm.

A FORTRAN program for computing the Steps 1 and 2 corrections is available at <[5]>.

7.1.3 Permanent deformation

The tidal model described above does contain in principle a time independent part so that the coordinates obtained by taking into account this model in the analysis will be "conventional tide free" values. (Note that they do *not* correspond to what would be observed in the absence of tidal perturbation. See the discussion in Chapter 1.) This section allows a user to compute "mean tide" coordinates from "conventional tide free" coordinates.

Specifically, the degree 2 zonal tide generating potential includes a spectral component of zero frequency and amplitude $H_0 = -0.31460$ m, and its effect enters the tidal displacement model through the time independent component of the expression (9). Evaluation of this component may be done using equations (5a) and (6) with $H_f = H_0, \theta_f = 0$, and with the same nominal values for the Love number parameters as were used in Step 1: $h_2 = 0.6078, l_2 = 0.0847$ along with $h^{(2)} = -0.0006$ and $l^{(2)} = 0.0002$. One finds the radial component of the permanent displacement according to (9) to be

$$[-0.1206 + 0.0001 P_2(\sin\phi)] P_2(\sin\phi) \text{ m}, \tag{18a}$$

and the transverse component to be

$$[-0.0252 - 0.0001 P_2(\sin\phi)] \sin 2\phi \text{ m} \tag{18b}$$

northwards, where $P_2(\sin\phi) = (3\sin^2\phi - 1)/2$.

These are the components of the vector to be added to the "conventional tide free" computed tide-corrected position to obtain the "mean tide" position. The radial component of this restitution to obtain the "mean tide" values amounts to about -12 cm at the poles and about $+6$ cm at the equator.

7.1.4 Rotational Deformation due to Polar Motion

The variation of station coordinates caused by the pole tide can amount to a couple of centimeters and needs to be taken into account.

Let us choose $\hat{x}, \hat{y}$ and $\hat{z}$ as a terrestrial system of reference. The $\hat{z}$ axis is oriented along the Earth's mean rotation axis, the $\hat{x}$ axis is in the direction of the adopted origin of longitude and the $\hat{y}$ axis is orthogonal to the $\hat{x}$ and $\hat{z}$ axes and in the plane of the 90° E meridian.

The centrifugal potential caused by the Earth's rotation is

$$V = \frac{1}{2}[r^2|\vec{\Omega}|^2 - (\vec{r}\cdot\vec{\Omega})^2], \tag{19}$$

[5] ftp://tai.bipm.org/iers/convupdt/chapter7/dehanttideinel.f

where $\vec{\Omega} = \Omega(m_1\ \hat{x} + m_2\ \hat{y} + (1 + m_3)\ \hat{z})$. Ω is the mean angular velocity of rotation of the Earth; m_1, m_2 describe the time dependent offset of the instantaneous rotation pole from the mean, and m_3, the fractional variation in the rotation rate; r is the geocentric distance to the station.

Neglecting the variations in m_3 which induce displacements that are below the mm level, the m_1 and m_2 terms give a first order perturbation in the potential V (Wahr, 1985)

$$\Delta V(r, \theta, \lambda) = -\frac{\Omega^2 r^2}{2} \sin 2\theta\, (m_1 \cos\lambda + m_2 \sin\lambda). \tag{20}$$

The radial displacement S_r and the horizontal displacements S_θ and S_λ (positive upwards, south and east respectively in a horizon system at the station) due to ΔV are obtained using the formulation of tidal Love numbers (Munk and MacDonald, 1960):

$$S_r = h_2 \frac{\Delta V}{g}, \qquad S_\theta = \frac{\ell_2}{g} \partial_\theta \Delta V, \qquad S_\lambda = \frac{\ell_2}{g} \frac{1}{\sin\theta} \partial_\lambda \Delta V. \tag{21}$$

The position of the Earth's mean rotation pole has a secular variation, and its coordinates in the Terrestrial Reference Frame discussed in Chapter 4 are given, in terms of the polar motion variables (x_p, y_p) defined in Chapter 5, by appropriate running averages $\bar{x}_p$ and $-\bar{y}_p$. Then

$$m_1 = x_p - \bar{x}_p, \qquad m_2 = -(y_p - \bar{y}_p). \tag{22}$$

For the most accurate results, estimates of the mean pole should be used. The IERS conventional mean pole is a linear model derived by the IERS Earth Orientation Centre from a fit over the period 1976–2000 of the data in <[6]>. It reads

$$\bar{x}_p(t) = \bar{x}_p(t_0) + (t - t_0)\dot{\bar{x}}_p(t_0), \quad \bar{y}_p = \bar{y}_p(t_0) + (t - t_0)\dot{\bar{y}}_p(t_0), \tag{23a}$$

$$\bar{x}_p(t_0) = 0.054, \quad \dot{\bar{x}}_p(t_0) = 0.00083, \quad \bar{y}_p(t_0) = 0.357, \quad \dot{\bar{y}}_p(t_0) = 0.00395, \tag{23b}$$

where $\bar{x}_p, \bar{y}_p$ are in arcseconds, their rates are in arcseconds per year, and t_0 is 2000.0 <[7]>.

Using Love number values appropriate to the frequency of the pole tide ($h_2 = 0.6207$, $l_2 = 0.0836$) and $r = a = 6.378 \times 10^6$m, one finds

$$\begin{aligned} S_r &= -33 \sin 2\theta\, (m_1 \cos\lambda + m_2 \sin\lambda)\ \text{mm}, \\ S_\theta &= -9 \cos 2\theta\, (m_1 \cos\lambda + m_2 \sin\lambda)\ \text{mm}, \\ S_\lambda &= 9 \cos\theta\, (m_1 \sin\lambda - m_2 \cos\lambda)\ \text{mm}, \end{aligned} \tag{24}$$

with m_1 and m_2 given in seconds of arc. Note that the values of the Love numbers include the anelastic contributions to the real part, which induce a contribution to the displacement of order 1 mm, but do not include the contributions to the imaginary part, which effects are about 5 times smaller. Taking into account that m_1 and m_2 vary, at most, 0.8 arcsec, the maximum radial displacement is approximately 25 mm, and the maximum horizontal displacement is about 7 mm. If X, Y, and Z are Cartesian coordinates of a station in a right-handed equatorial coordinate system, the changes in them due to polar motion are (note that the order of components is different in equations (24) and (25))

$$[dX, dY, dZ]^T = R^T [S_\theta, S_\lambda, S_r]^T, \tag{25}$$

where

$$R = \begin{pmatrix} \cos\theta\cos\lambda & \cos\theta\sin\lambda & -\sin\theta \\ -\sin\lambda & \cos\lambda & 0 \\ \sin\theta\cos\lambda & \sin\theta\sin\lambda & \cos\theta \end{pmatrix}. \tag{26}$$

[6] ftp://tai.bipm.org/iers/conv2003/chapter7/annual.pole

[7] Note that the original data used to generate the linear model uses Besselian epochs thus, strictly speaking, the time argument t in (23a) is also a Besselian epoch. However, for all practical purposes, a Julian epoch may be used for t.

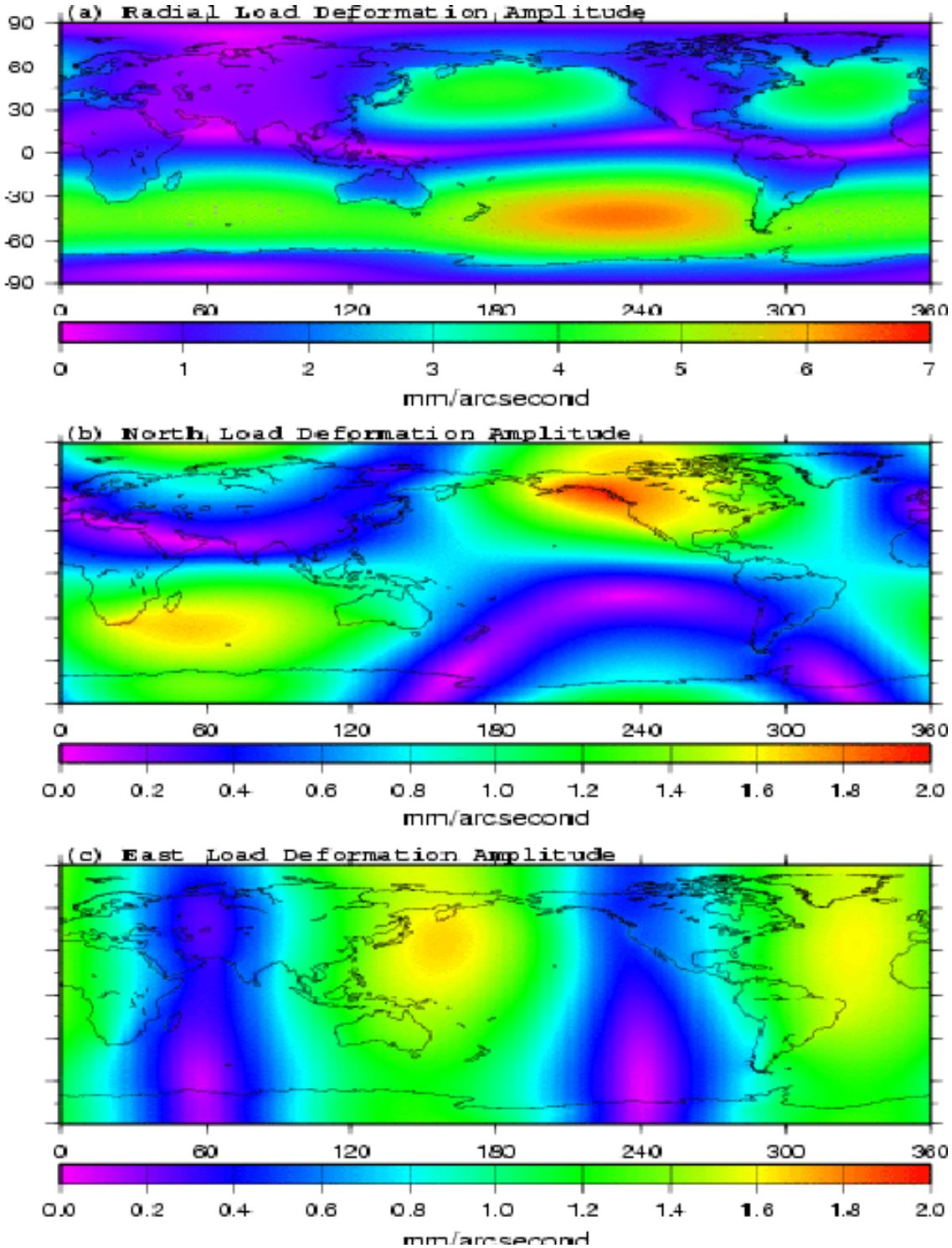

Fig. 7.1 Loading from ocean pole tide: Amplitude as a function of the amplitude of wobble variable.

7.1.5 Ocean Pole Tide Loading

The ocean pole tide is generated by the centrifugal effect of polar motion on the oceans. This centrifugal effect is defined in equation (10) from section 6.2. Polar motion is dominated by the 14-month Chandler wobble and annual variations. At these long periods, the ocean pole tide is expected to have an equilibrium response, where the displaced ocean surface is in equilibrium with

the forcing equipotential surface.

Desai (2002) presents a self-consistent equilibrium model of the ocean pole tide. This model accounts for continental boundaries, mass conservation over the oceans, self-gravitation, and loading of the ocean floor. Using this model, the load of the ocean pole tide produces the following deformation vector at any point on the surface of the Earth with latitude ϕ and longitude λ. The load deformation vector is expressed here in terms of radial, north and east components, u_r, u_n, and u_e, respectively, and is a function of the wobble parameters (m_1, m_2).

$$\begin{bmatrix} u_r(\phi,\lambda) \\ u_n(\phi,\lambda) \\ u_e(\phi,\lambda) \end{bmatrix} = K \left\{ (m_1\gamma_2^R + m_2\gamma_2^I) \begin{bmatrix} u_r^R(\phi,\lambda) \\ u_n^R(\phi,\lambda) \\ u_e^R(\phi,\lambda) \end{bmatrix} + (m_2\gamma_2^R - m_1\gamma_2^I) \begin{bmatrix} u_r^I(\phi,\lambda) \\ u_n^I(\phi,\lambda) \\ u_e^I(\phi,\lambda) \end{bmatrix} \right\} \qquad (27)$$

where

$$K = \frac{4\pi G a_E \rho_w H_p}{3 g_e}$$

$$H_p = \left[\frac{8\pi}{15}\right]^{1/2} \frac{\Omega^2 a_E^4}{GM}$$

and
Ω, a_E, GM, g_e, and G are defined in Chapter 1,
ρ_w = density of sea water = 1025 kgm^{-3},
$\gamma = (1 + k_2 - h_2) = \gamma_2^R + i\gamma_2^I = 0.6870 + i0.0036$ (Values of k_2 and h_2 appropriate for the pole tide are as given in sections 6.2 and 7.1.4),
(m_1, m_2) are the wobble parameters. Refer to sub-section 7.1.4 for the relationship between the wobble variables (m_1, m_2) and the polar motion variable (x_p, y_p).
$u_r^R(\phi,\lambda)$, $u_n^R(\phi,\lambda)$, $u_e^R(\phi,\lambda)$ are the real part of the ocean pole load tide coefficients.
$u_r^I(\phi,\lambda)$, $u_n^I(\phi,\lambda)$, $u_I^R(\phi,\lambda)$ are the imaginary part of the ocean pole load tide coefficients.

Maps of the required ocean pole load tide coefficients are available on an equally spaced 0.5 by 0.5 degree global grid at <[8]>. These coefficients provide the surface deformations with respect to the instantaneous center of mass of the deformed Earth including the mass of the loading ocean pole tide.

The amplitude of this loading deformation is shown in Figure 7.1 in mm per arcsecond as a function of the amplitude m of the wobble components (m_1, m_2). Given that the amplitude of the wobble variable is typically of order 0.3 arcseconds, the load deformation is typically no larger than about (1.8, 0.5, 0.5) mm in (radial, north, east) components, but it may occasionally be larger.

7.1.6 Atmospheric Loading

Temporal variations in the geographic distribution of atmospheric mass load the Earth and deform its surface. For example, pressure variations on the order of 20 hPa (and even larger) at mid-latitudes, are observed in synoptic pressure systems with length scales for 1000–2000 km and periods of approximately two weeks. Seasonal pressure changes due to air mass movements between the continents and oceans can have amplitudes of up to 10 hPa in particular over the large land masses of the Northern Hemisphere. At the interannual periods, basin-wide air pressure signals with amplitudes of several hPa also contribute to the spectrum of the loading signal.

Other surface loads due to changes in snow and ice cover, soil moisture and groundwater, as well as ocean-bottom pressure also contribute to surface displacements. For example, at seasonal time scales, it is expected that the contribution of hydrological loads to surface displacements exceeds the one from air pressure (Blewitt *et al.*, 2001). However, while the atmospheric load is fairly well known from global air pressure data sets, no suffcient models for ocean bottom pressure, snow and soil moisture exists at this time. Therefore, in the following, focus is on atmospheric loading. However, the discussion applies also to any other surface load.

Theoretical studies by Rabbel and Zschau (1985), Rabbel and Schuh (1986), vanDam and Wahr (1987), and Manabe *et al.* (1991) demonstrate that vertical crustal displacements of up to 25

[8] ftp://tai.bipm.org/iers/convupdt/chapter7/opoleloadcoefcmcor.txt

mm are possible at mid-latitude stations due to synoptic pressure systems. Annual signals in the vertical are on the order of 1–2 mm but maximum signals of more than 3 mm are possible over large parts of Asia, Antarctica, Australia and Greenland (Mangarotti *et al.*, 2001; Dong *et al.*, 2002). Pressure loading effects are larger at higher latitude sites due to the more intensive weather systems (larger in amplitude and more spatially coherent) found there. Effects are smaller at mid-latitude sites and at locations within 500 km of the sea or ocean due to the inverted barometer response of the ocean. In all cases, horizontal crustal deformations are about one-third the amplitude of the vertical effects.

Two basic methods for computing atmospheric loading corrections to geodetic data have been applied so far: 1) using geophysical models or simple approximations derived from these models and 2) using empirical models based on site-dependent data.

The standard geophysical model approach is based on the estimation of atmospheric loading effects (vertical and horizontal deformations, gravity, tilt and strain) via the convolution of Green's functions with a global surface pressure field. The geophysical approach is analogous to methods used to calculate ocean tidal loading effects. However, due to the continuous spectrum of the atmospheric pressure variations, the compution of the atmospheric loading signal must be carried out in the time domain. The major advantage of the geophysical model approach is that loading effects can be computed in a standardized way for any point on the Earth's surface more or less instantaneously. The geophysical approach currently suffers from a number of problems including: the requirement of a global pressure data set, a minimum of 24 hours in time delay in the availability of the global pressure data set, limitations of the pressure data itself (low temporal and spatial resolution), uncertainties in the Green's functions and uncertainties in the ocean response model.

In the empirical approach, site-dependent pressure loading effects are computed by determining the fit of local pressure variations to the geodetic observations of the vertical crustal motion. This approach is likely to produce better results (than the geophysical approach) for a given site but has a number of drawbacks as well. 1.) Geodetic observations have to be available for a certain period of time before a reliable regression coeffcient can be determined; this period of time may be as large as serveral years. 2.) The regression coefficients cannot be extraploated to a new site (for which no data exist); 3.) The regression coefficient has been observed to change with time and with observing technique; 4.) Regression coefficients at coastal sites are time dependent due to interannual changes in the regional weather pattern (H.-P. Plag, personal communication, 2002); 5.) The regession coefficient can only be used for vertical crustal motions; and 6.) It is uncertain that other pressure correlated geodetic signals are not being 'absorbed' into the regression coefficient determination. So while this approach would lower the scatter on a given geodetic time series the most, one would always be uncertain whether only atmospheric loading effects were being removed with the correlation coefficient.

In a hybrid method, regression coefficients determined from a geophysical model instead of geodetic observations could be used to operationally correct observed vertical position determinations from local air pressure alone. The vertical deformation caused by the change in pressure, in this case, can then be given in terms of a local pressure anomaly. The regression coefficients can be determined by fitting local pressure to the vertical deformation predicted by the geophysical model. Regression coefficients determined in this manner would still suffer from both the uncertainty in the Green's function and the quality of the air pressure data.

In February 2002, the Special Bureau on Loading (SBL) was established within the IERS. The charge of the SBL is to promote, stimulate and coordinate work and progress towards a service providing information on Earth surface deformation due to surface mass loading, including the atmosphere, ocean and continental hydrosphere. In establishing the SBL the IERS is recommending that the convention for computing atmospheric loading corrections will be based on the geophysical model approach.

At the 2002 IERS Meeting in Munich, the IERS adopted the convention that corrections for surface load variations including the atmosphere should be determined using the geophysical model approach. Further, these corrections should be obtained from the IERS SBL. The point of this recommendation is to ensure that comparisons of geodetic time series between different observing techniques or within the same technique but at different times and locations have a consistent

atmospheric pressure loading (and later also non-tidal ocean and continental hydrological loading) correction applied.

The ultimate goal of the SBL is to provide in near real-time a consistent global solution data set, describing at the surface, deformation due to all surface loads (including atmospheric pressure variations) in reference frames relevant for direct comparison with geodetic observing techniques. The SBL will provide global gridded solutions of 3-D displacements and time series of displacements for all IERS sites. Time series will be determined from 1985 to the present. Displacements will be determined for both the European Center for Medium Range Weather Forecasts and the National Center for Environmental Prediction operational pressure data sets for the inverted barometer and the non-inverted barometer ocean models. For more information see: <[9]>.

Regression coefficients based on a geophysical model are already available for a number of VLBI sites through the SBL web page and the IERS Convention's web page <[10]>. The regression coefficients were computed using 18 years of the NCEP Reanalysis Data (1 Jan. 1980 to 31 Dec. 1997). The data are 6 hourly values of surface pressure given on a 2.5°×2.5° global grid. Vertical crustal motions at a particular site are modeled by convolving Farrell's (1972) Greens functions for a Gutenberg-Bullen A Earth model. The ocean was assumed to be inverse barometric for the calculations. The regression results (mm/mbar) are determined via a linear regression between the modeled crustal displacements and the local surface pressure determined from the NCEP data set. An inverted barometer model was used in determining the ocean's response to pressure.

For more information on atmospheric pressure loading and geodetic time series, see the references listed in the extended bibliography.

7.2 Displacement of Reference Points of Instruments

7.2.1 VLBI Antenna Thermal Deformation

The following has been excerpted from the Explanatory Supplement to the IERS Conventions (1996) Chapters 6 and 7 (Schuh, 1999).

Most VLBI telescopes are of Cassegrain type with alt-azimuth or polar mount and secondary focus. Figures 7.2 and 7.3, based on Nothnagel *et al.* (1995), show the principles of these antenna mounts. The height of the concrete foundation is denoted by h_f, the height of the antenna pillar by h_p, the height of the vertex by h_v, the height of the subreflector by h_s and the declination shaft by h_d.

Then, the thermal deformation effect $\Delta\tau$ in s on the VLBI delay measurement τ can be modeled. For alt-azimuth mounts

$$\begin{aligned}\Delta\tau &= \tfrac{1}{c}\cdot\Big[\gamma_f\cdot(T(t-\Delta t_f)-T_0)\cdot(h_f\cdot\sin(\varepsilon))\\ &\quad +\gamma_a\cdot(T(t-\Delta t_a)-T_0)\cdot(h_p\cdot\sin(\varepsilon)+h_v-1.8\cdot h_s)\Big].\end{aligned} \tag{28}$$

For polar mounts

$$\begin{aligned}\Delta\tau &= \tfrac{1}{c}\cdot\Big[\gamma_f\cdot(T(t-\Delta t_f)-T_0)\cdot(h_f\cdot\sin(\varepsilon))\\ &\quad +\gamma_a\cdot(T(t-\Delta t_a)-T_0)\cdot(h_p\cdot\sin(\varepsilon)\\ &\quad +h_v-1.8\cdot h_s+h_d\cdot\cos(\delta))\Big].\end{aligned} \tag{29}$$

In the above equations (28) and (29) c in m/s is the speed of light, γ_f and γ_a in $1/^\circ C$ are the expansion coefficents for the foundation and for the antenna, respectively, and h_f, h_p, h_v, h_s and h_d are the dimensions of the telescopes in m. For prime focus antennas, the factor for h_s is 0.9 instead of 1.8. The temperature of the telescope structure is denoted by T, and T_0 is a reference temperature, *e.g.* 20°C which is the usual reference temperature used when designing and constructing buildings. If the actual temperature of the telescope structure is not available, which might be the case at most VLBI sites, the surrounding air temperature can be taken instead.

[9] http://www.gdiv.statkart.no/sbl
[10] ftp://maia.usno.navy.mil/conv2000/chapter7/atmospheric.regr

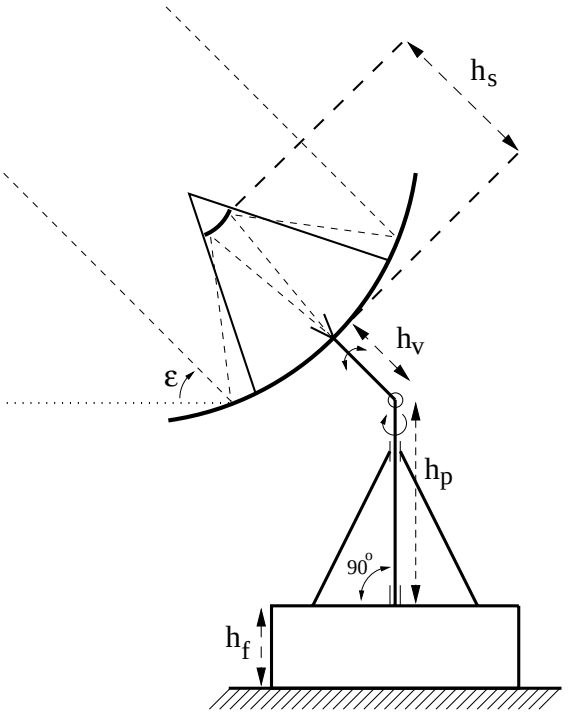

Fig. 7.2 Alt-azimuthal telescope mount.

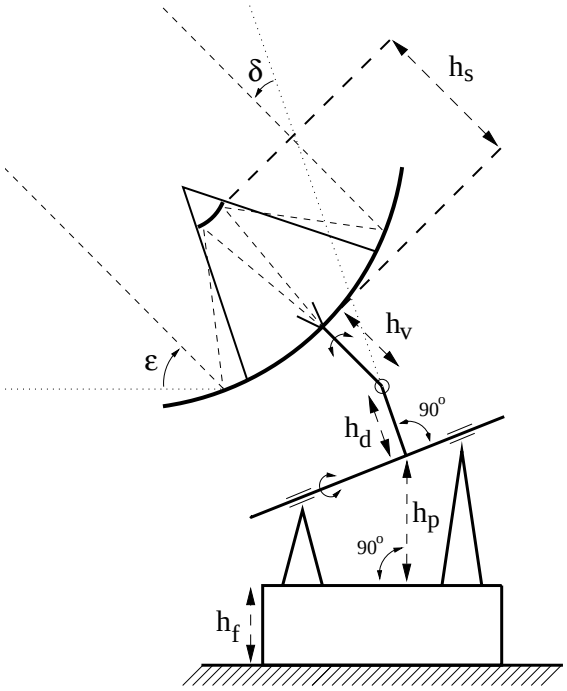

Fig. 7.3 Polar telescope mount.

The time delay between the change in the surrounding air temperature and the expansion of the telescope structure is denoted by Δt_f for the foundation and by Δt_a for the antenna and depend strongly on the material of the telescope. Measurements yielded values of Δt_a=2 hours for a steel telescope structure (Nothnagel *et al.*, 1995) and of Δt_f=6 hours for a concrete telescope structure (Elgered and Carlsson, 1995). The elevation and declination of the observed radio source are denoted by ε and δ.

Table 7.6 Dimensions and expansion coefficients of frequently used geodetic VLBI telescopes.

Telescope	Foundation part (concrete)		Antenna part (steel)				
	h_f	γ_f	h_p	h_v	h_s	h_d	γ_a
	m	$1/°C$	m	m	m	m	$1/°C$
Effelsberg	0.0	1.0×10^{-5}	50.0	8.5	28.0	–	1.2×10^{-5}
Hartebeesthoek	0.0	1.0×10^{-5}	12.7	2.3	9.4	6.7	1.2×10^{-5}
Madrid	3.0	1.0×10^{-5}	16.8	2.7	10.8	–	1.2×10^{-5}
Matera	3.0	1.0×10^{-5}	10.5	3.8	5.7	–	1.2×10^{-5}
Medicina	2.3	1.0×10^{-5}	15.5	4.3	4.3	–	1.2×10^{-5}
Noto	2.2	1.0×10^{-5}	15.7	4.2	5.0	–	1.2×10^{-5}
O'Higgins	1.0	1.0×10^{-5}	6.2	–	–	–	1.2×10^{-5}
Onsala	11.3	1.0×10^{-5}	2.9	3.4	5.5	–	1.2×10^{-5}
Westford	16.9	1.0×10^{-5}	2.0	3.0	3.6	–	1.2×10^{-5}
Wettzell	8.0	1.0×10^{-5}	4.0	3.7	7.9	–	1.2×10^{-5}

Table 7.6 contains the dimensions of some frequently used geodetic VLBI antennas and mean expansion coefficients.

Table 7.7 gives the thermal variation $\Delta\tau$ of the VLBI delay observable, based on the telescope dimensions and expansion coefficients given in Table 7.6 and equations (28) and (29). Temperature variation $(T - T_0)$ of 10°C and radio source elevations between 5° and 90° were entered, time lags

Table 7.7 Thermal variations $\Delta\tau$ in ps of the VLBI delay observable for frequently used geodetic VLBI telescopes for a temperature variation of 10°C and different radio source elevations.

Telescope	$(T - T_0)$=10°C Elevation ε			
	5°	30°	60°	90°
	$\Delta\tau$	$\Delta\tau$	$\Delta\tau$	$\Delta\tau$
	ps	ps	ps	ps
Effelsberg	−15.0	−6.8	+0.6	+3.2
Hartebeesthoek	−7.8	−5.0	−1.9	+0.1
Madrid	−6.0	−2.8	0.0	+1.0
Matera	−2.1	0.0	+1.9	+2.6
Medicina	−0.8	+2.1	+4.6	+5.6
Noto	−1.3	+1.6	+4.2	+5.1
O'Higgins	0.2	+1.4	+2.4	+2.8
Onsala	−2.2	−0.1	+1.7	+2.3
Westford	−0.8	+1.8	+4.2	+5.0
Wettzell	−3.8	−2.0	−0.5	0.0

Δt_f and Δt_a were assumed to be zero.

For big VLBI telescopes, variations in the VLBI delay observations of several picoseconds can occur. Regarding a baseline of two telescopes with the signal from the radio source arriving first at site 1, the total effect on the measured delay on the baseline is:

$$\Delta\tau_{baseline} = \Delta\tau_1 - \Delta\tau_2.$$

References

Blewitt, G., Lavallée, D., Clarke, P., and Nurutdinov, K., 2001, "A new global mode of the Earth deformation: Seasonal cycle detected," *Science*, **294**, pp. 2342–2345.

Bos, M. S., 2005, personnal communication.

Cartwright, D. E. and Tayler, R. J., 1971, "New Computations of the Tide-Generating Potential," *Geophys. J. Roy. astr. Soc.*, **23**, pp. 45–74.

Cartwright, D. E. and Edden, A. C., 1973, "Corrected Tables of Tidal Harmonics," *Geophys. J. Roy. astr. Soc.*, **33**, pp. 253–264.

Chelton, D. B. and Enfield, D. B., 1986, "Ocean Signals in Tide Gauge Records," *J. Geophys. Res.*, **91**, pp. 9081–9098.

Desai, S. D., 2002, "Observing the pole tide with satellite altimetry," *J. Geophys. Res.*, **107**(C11), 3186, doi:10.1029/ 2001JC001224.

Dong, D., Fang, P., Bock, Y., Cheng, M. K., and Miyazaki, S., 2002, "Anatomy of apparent seasonal variations from GPS-derived site position time series," *J. Geophys. Res.*, **107(B4)**, ETG 9-1–9-8.

Doodson, A. T., 1928, "The Analysis of Tidal Observations," *Phil. Trans. Roy. Soc. Lond.*, **227**, pp. 223–279.

Eanes, R. J., 1994, "Diurnal and semidiurnal tides from TOPEX/POSEIDON altimetry," paper G32B-6, presented at the Spring Meeting of the AGU, Baltimore, MD, *EOS Trans AGU*, **75**, p. 108.

Eanes R. J. and Bettadpur, S., 1995, "The CSR 3.0 global ocean tide model," *Technical Memorandum CSR-TM-95-06*, Center for Space Research, University of Texas, Austin, TX.

Egbert, G. D., Bennett, A. F., and Foreman, M. G. G. , 1994, "TOPEX/ POSEIDON tides estimated using a global inverse model," *J. Geophys. Res.*, **99**, pp. 24,821–24,852.

Egbert, G. D., Erofeeva, S.Y. , 2002, "Efficient inverse modeling of barotropic ocean tides," *J. Atmos. Ocean. Technol.*, **19(2)**, pp. 183–204.

Elgered, G. and Carlsson, T. R., 1995, "Temperature Stability of the Onsala 20-m Antenna and its Impact on Geodetic VLBI," *Proc. of the 10th Working Meeting on European VLBI for Geodesy and Astrometry*, Lanotte, R. and Bianco, G. (eds.), Matera, pp. 69–78.

Farrell, W. E., 1972, "Deformation of the Earth by Surface Loads," *Rev. Geophys. Space Phys.*, **10**, pp. 761–797.

Haas, R., 1996, "Untersuchungen zu Erddeformationsmodellen fur die Auswertung von geodatischen VLBI-Messungen", PhD Thesis, Deutsche Geodatische Kommission, Reihe C, Heft Nr. 466, 103 pp.

Haas, R., Scherneck, H.-G., and Schuh, H., 1997, "Atmospheric loading corrections in Geodetic VLBI and determination of atmospheric loading coefficients," in *Proc. of the 12 Working Meeting on European VLBI for Geodesy and Astronomy*, Pettersen, B.R. (ed.), Honefoss, Norway, 1997, pp. 122–132.

Hartmann, T. and Wenzel, H.-G., 1995, "The HW95 Tidal Potential Catalogue," *Geophys. Res. Lett.*, **22**, pp. 3553–3556.

Hugentobler, U., 2006, personnal communication.

Le Provost, C., Genco, M. L., Lyard, F., Incent, P., and Canceil, P., 1994, "Spectroscopy of the world ocean tides from a finite element hydrological model," *J. Geophys. Res.*, **99**, pp. 24777–24798.

Le Provost, C., Lyard, F., Molines, J. M., Genco, M. L., and Rabilloud, F., 1998, "A hydrodynamic ocean tide model improved by assimilating a satellite altimeter-derived data set," *J. Geophys. Res.*, **103(C3)**, pp. 5513–5529.

Lefèvre, F., Lyard, F. H., and Le Provost, C. , 2000, "FES98: A new global tide finite element solution independent of altimetry," *Geophys. Res. Lett.*, **27(17)**, pp. 2717–2720.

Lefèvre, F., Lyard, F., Le Provost, C., and Schrama, E.J.O., 2002, "FES99: A Global Tide Finite Element Solution assimilating Tide Gauge and Altimetric Information," *Journal of Atmospheric and Oceanic Technology*, **19**, pp. 1345-1356.

Letellier, T., 2004, "Etude des ondes de marée sur les plateaux continentaux," Thèse doctorale, Université de Toulouse III, 237pp.

MacMillan, D. S. and Gipson, J. M., 1994, "Atmospheric Pressure Loading Parameters from Very Long Baseline Interferometry Observations," *J. Geophys. Res.*, **99**, pp. 18081–18087.

Manabe, S. T., Sato, T., Sakai, S., and Yokoyama, K., 1991, "Atmospheric Loading Effects on VLBI Observations," in Proc. of the AGU Chapman Conference on Geodetic VLBI: Monitoring Global Change, *NOAA Tech. Rep. NOS 137 NGS 49*, pp. 111–122.

Mangiarotti, S., Cazenave A., Soudarin L., and Cretaux J. F., 2001, "Annual vertical crustal motions predicted from surface mass redistribution and observed by space geodesy," *J. Geophys. Res.*, **106**, pp. 4277–4291.

Mathers, E. L. and Woodworth, P. L., 2001, "Departures from the local inverse barometer model observed in altimeter and tide gauge data and in a global barotropic numerical model," *J. Geophys. Res.*, **106**, pp. 6957–6972.

Mathews, P. M., Buffett, B. A., and Shapiro, I. I., 1995, "Love numbers for a rotating spheroidal Earth: New definitions and numerical values," *Geophys. Res. Lett.*, **22**, pp. 579–582.

Matsumoto, K., Takanezawa, T. and Ooe, M., 2000, "Ocean Tide Models Developed by Assimilating TOPEX/POSEIDON Altimeter Data into Hydrodynamical Model: A Global Model and a Regional Model Around Japan," *J. Oceanog.*, **56**, pp. 567–581.

Munk, W. H. and MacDonald, G. J. F., 1960, *The Rotation of the Earth*, Cambridge Univ. Press, New York, pp. 24–25.

Nothnagel, A., Pilhatsch, M., and Haas, R., 1995, "Investigations of Thermal Height Changes of Geodetic VLBI Radio Telescopes," in *Proceedings of the 10th Working Meeting on European VLBI for Geodesy and Astrometry*, Lanotte, R. and Bianco, G. (eds.), Matera, pp. 121–133.

Ponte, R. M., Salstein, D. A., and Rosen, R. D., 1991, "Sea Level Response to Pressure Forcing in a Barotropic Numerical Model," *J. Phys. Oceanogr.*, **21**, pp. 1043–1057.

Rabbel, W. and Schuh, H., 1986, "The Influence of Atmospheric Loading on VLBI Experiments," *J. Geophys.*, **59**, pp. 164–170.

Rabbel, W. and Zschau, J., 1985, "Static Deformations and Gravity Changes at the Earth's Surface due to Atmospheric Loading," *J. Geophys.*, **56**, pp. 81–99.

Ray, R., 1999, "A Global Ocean Tide Model From TOPEX/POSEIDON Altimetry: GOT99.2," *NASA Technical Memorandum, NASA/TM-1999-209478*, National Aeronautics and Space Administration, Goddard Space Flight Center, Greenbelt, MD.

Row, L. W., Hastings, D. A., and Dunbar, P. K., 1995, "TerrainBase Worldwide Digital Terrain Data," NOAA, National Geophysical Data Center, Boulder CO.

Scherneck, H.-G., 1990, "Loading Green's functions for a continental shield with a Q-structure for the mantle and density constraints from the geoid," *Bull. d'Inform. Marées Terr.*, **108**, pp. 7757–7792.

Scherneck, H.-G., 1991, "A Parameterized Solid Earth Tide Model and Ocean Tide Loading Effects for Global Geodetic Baseline Measurements," *Geophys. J. Int.*, **106**, pp. 677–694.

Scherneck, H.-G., 1993, "Ocean Tide Loading: Propagation of Errors from the Ocean Tide into Loading Coefficients," *Man. Geod.*, **18**, pp. 59–71.

Scherneck, H.-G., 1999, in *Explanatory Supplement to the IERS Conventions (1996) Chapters 6 and 7*, Schuh, H. (ed.), DGFI Report 71, pp. 19–23.

Schuh, H. (ed.), 1999, *Explanatory Supplement to the IERS Conventions (1996) Chapters 6 and 7*, DGFI Report 71.

Schwiderski, E. W. and Szeto, L. T., 1981, "The NSWC global ocean tide data tape (GOTD), its features and application, random-point tide program," *NSWC-TR 81–254*, Naval Surface Weapons Center, Dahlgren, VA, 19 pp.

Sun, H. P., Ducarme, B., and Dehant, V., 1995, "Effect of the Atmospheric Pressure on Surface Displacements," *J. Geod.*, **70**, pp. 131–139.

Tamura, Y., 1987, "A harmonic development of the tide-generating potential," *Bull. d'Inform. Marées Terr.*, **99**, pp. 6813–6855.

vanDam, T. M. and Wahr, J. M., 1987, "Displacements of the Earth's Surface due to Atmospheric Loading: Effects on Gravity and Baseline Measurements," *J. Geophys. Res.*, **92**, pp. 1281–1286.

vanDam, T. M. and Herring, T. A., 1994, "Detection of Atmospheric Pressure Loading Using Very Long Baseline Interferometry Measurements," *J. Geophys. Res.*, **99**, pp. 4505–4517.

vanDam, T. M., Blewitt, G., and Heflin, M. B., 1994, "Atmospheric Pressure Loading Effects on Global Positioning System Coordinate Determinations," *J. Geophys. Res.*, **99**, pp. 23,939–23,950.

Wahr, J. M., 1981, "The Forced Nutations of an Elliptical, Rotating, Elastic, and Oceanless Earth," *Geophys. J. Roy. astr. Soc.*, **64**, pp. 705–727.

Wahr, J. M., 1985, "Deformation Induced by Polar Motion," *J. Geophys. Res.*, **90**, pp. 9363–9368.

Wahr, J. M. and Sasao, T., 1981, "A diurnal resonance in the ocean tide and the Earth's load response due to the resonant free "core nutation"," *Geophys. J. R. astr. Soc.*, **64**, pp. 747–765.

Wenzel, H.-G., 1996 "The nanogal software: Earth tide data processing package ETERNA 3.30," *Bulletin d'Informations Marées Terrestres*, **124**, pp. 9425–9439.

Wessel, P. and Smith, W. H. F., 1998, "New, improved version of the Generic Mapping Tools released," *EOS Trans. AGU*, **79**, 579.

Zschau, J., 1983, "Rheology of the Earth's mantle at tidal and Chandler Wobble periods," *Proc. Ninth Int. Symp. Earth Tides*, New York, 1981, Kuo, J. T. (ed.), Schweitzerbart'sche Verlagsbuchhandlung, Stuttgart, pp. 605–630.